Photonic-Crystal Like Approach to Structural Color of the Earthworm Epidermis

Tsuyoshi Ueta[1*], Yoshihiro Otani[2] and Naoshi Nishimura[2]

[1]*Institute of Media and Information Technology, Chiba University, 1-33 Yayoi-cho, Inage-ku, Chiba 263-8522, Japan*
[2]*Graduate School of Informatics, Kyoto University, Yoshida Honmachi, Sakyo-ku, Kyoto 606-8501, Japan*
[*]*E-mail address: tsuyoshi_ueta@jikei.ac.jp*

(Received December 3, 2010; Accepted August 16, 2012)

The epidermis of an earthworm has a log-pile structure of fibers, and exhibits a structural color. The structure is considered as a photonic crystal. Optical properties of the epidermis of an earthworm have been investigated numerically by means of the analogy of the photonic crystal. The numerical method employed here is the periodic fast multipole method. The structural color is reproduced with the RGB color from the reflection spectrum. The reflection spectrum and the reproduced color are compared with those by a multilayer model and it is confirmed that the treatment as a photonic crystal is important.

Key words: Earthworm Epidermis, Structural Color, Photonic Crystal, Log-pile Structure, Periodic FMM

1. Introduction

Some kinds of creatures assume a beautiful color as shown in Fig. 1. In particular, the structural color is used for coloring in birds and Insecta (Kinoshita *et al.*, 2002a, b; Vukusic and Sambles, 2003; Kinoshita and Yoshioka, 2005). The color is for mimicking, for warning to their predators and for attracting females. It is, of course, effective and used just in light. Nonetheless, it is known that annelids, such as an earthworm, a mussel worm, etc. which live in the eclipsed ground and are considered to be unrelated to a color, shine blue to the incidence light of a certain angle as shown in Fig. 2(a) (Kosaku and Miyamoto, 2002a, b). Miyamoto and Kosaku (2005) found out a structure assuming a structural color on the epidermis of an earthworm (*Metaphire communissima* (Goto and Hatai, 1899)) as shown in Fig. 2(b) (Miyamoto and Kosaku, 2005). The structure exists in the vitric membrane of epidermis. It is the structure stacked 15–20 layers, rotating lattice structures 90° by turns, where a lattice structure consists of the vitric fibers of 108–183 nm in diameter located in parallel at intervals of 86–200 nm. They have proposed modeling the stacked structure by a log-pile structure of fibers as shown in Fig. 3.

Furthermore, they approximated a layer which consists of fibers arranged at equal intervals in parallel, by a film with an effective dielectric constant of the average of that of the layer, and they modeled the log-pile structure as a multilayer of the effective film. It was, then, shown that the Bragg wavelength of the multilayer film is well in agreement with the observed wavelength of the structural color.

On the other hand, the structural color of the wing of a butterfly is analyzed considering the wing as a photonic crystal (Nishiyama *et al.*, 2000; Kinoshita *et al.*, 2002a, b; Biró *et al.*, 2003). Since the log-pile structure of vitric fiber is a typical photonic crystal, we should analyze the optical property of this system theoretically and numerically by treating it as a photonic crystal properly (Joannopoulos *et al.*, 1995). The purpose of the present paper is to perform it. Furthermore, the structural color which the epidermis assumes is reproduced by converting the reflection spectrum of the model and composing RGB color.

2. Numerical Method and Numerical Model

In this research, according to Miyamoto and Kosaku (2005), the epidermis of an earthworm is modeled as periodical structure of cylindrical glass rods like Fig. 3. The problem that a plane wave of electromagnetic waves enters toward the periodical structure is considered, and the relation between incident wavelength and energy reflectance, namely, a reflection spectrum, is calculated to various incident angles. In treatment of such a system, it is necessary to deal with the Maxwell equation as the governing equation in the full vector formulation (Joannopoulos *et al.*, 1995). For solving this equation, numerical computation is indispensable.

Although the vector KKR for the periodic system of cylindrical rods can perform the numerical computation most in a short time (Ohtaka *et al.*, 1998), in this research, the periodic fast multipole method with higher flexibility (periodic FMM) is employed. In general, when the Maxwell equations are numerically solved in a large-scale system, the fast multipole method, which is the boundary element method to which multipole expansion is applied, is well used, where, in the boundary element method, the differential equations, i.e., the Maxwell equations, are transformed into an integral equation by means of a tensor Green function. The periodic FMM is a numerical method whose

Copyright © Society for Science on Form, Japan.

*Present address: The Jikei University School of Medicine Physics Laboratory, 8-3-1 Kokuryo-cho, Chofu, Tokyo 182-8570, Japan.

Fig. 1. Structural color of a morpho butterfly.

(a)

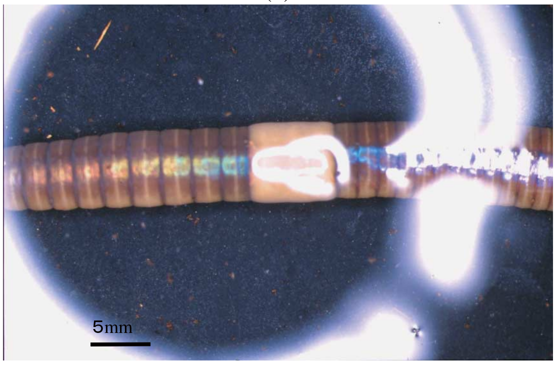

(b)

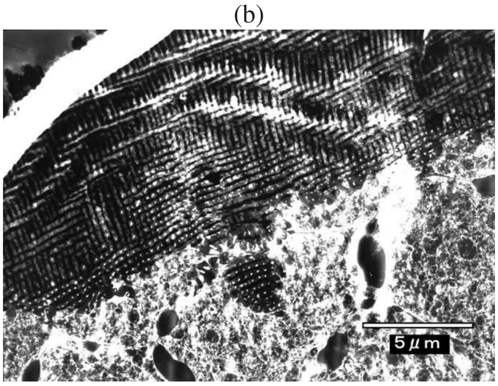

Fig. 2. (a) Structural color of an earthworm (*Metaphire communissima* (Goto and Hatai, 1899)). (b) A TEM image of a parallel section of the glass membrane of the earthworm. Both images are reproduced from (Kosaku and Miyamoto, 2002a).

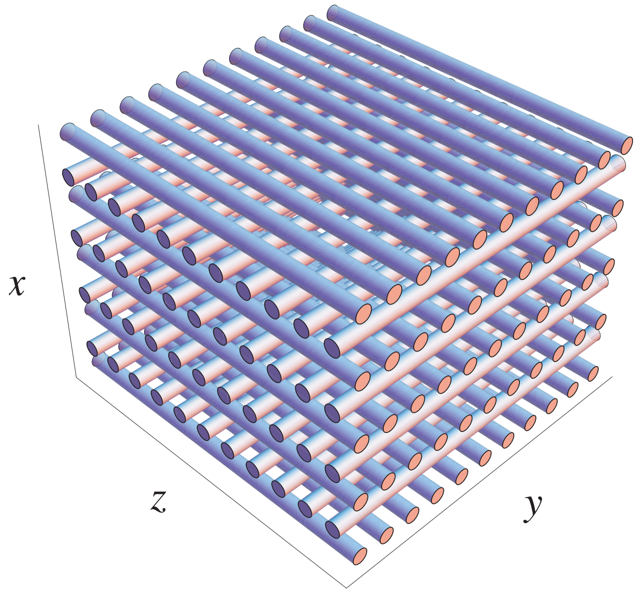

Fig. 3. A model of the epidermis of an earthworm, called a log-pile structure of fibers.

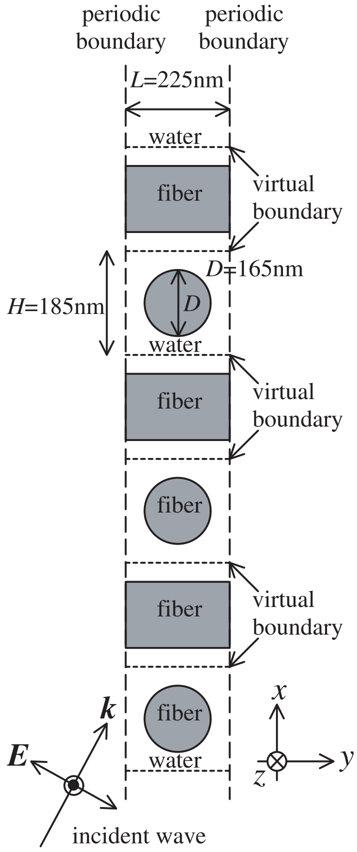

Fig. 4. The unit cell of the periodical structure in two directions of 6 layers in the water.

Green function is extended for the case that scattering domains exist periodically in a system (Otani and Nishimura, 2008).

In the periodic FMM, a system which is finite in the direction stacking layers, i.e., x-direction, but infinite in the y- and z-directions is considered. The unit cell of the periodical structure in two directions of six layers in the water is defined as shown in Fig. 4.

By referring to table 1 of Miyamoto and Kosaku (2005), the values of the interval L of a fiber, the layer space H, and the diameter D of a fiber are estimated as $D = 165$ nm, $H = 185$ nm and $L = 225$ nm, respectively. The refractive index of water and the fiber is set to $n_1 = 1.33$ and $n_2 = 1.58$, respectively. The relative dielectric constant of water and the fiber are, then, $\varepsilon_1 = 1.7689$ and $\varepsilon_2 = 2.4964$, respectively, and both relative permeabilities are set to $\mu_1 = \mu_2 = 1$.

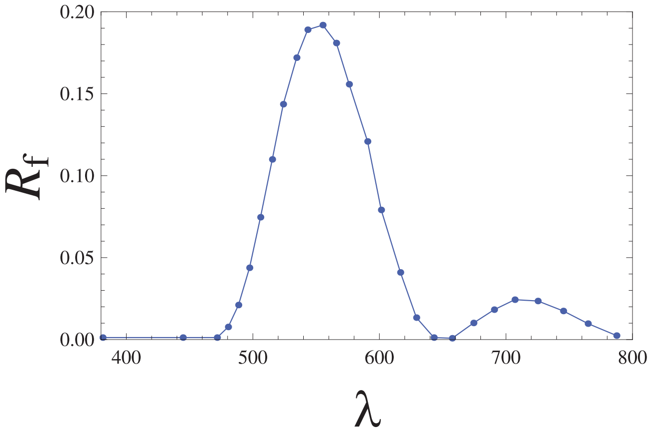

Fig. 5. The energy reflection spectrum for $\phi = 0°$.

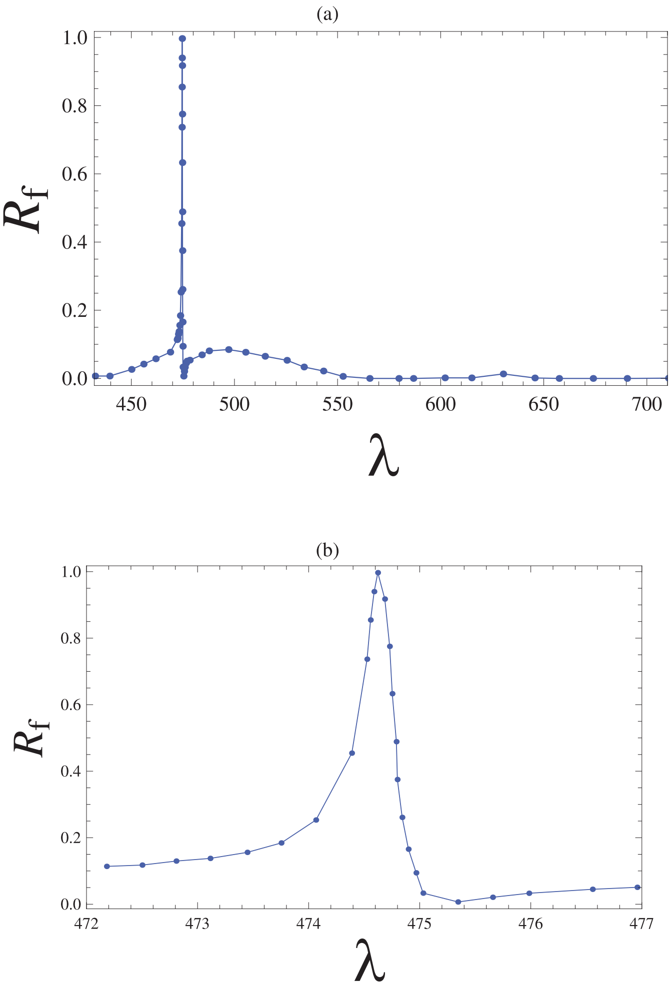

Fig. 6. (a) The energy reflection spectrum for $\phi = 30°$. (b) Magnification around the sharp peak.

In the present study, an incident magnetic field is concretely given as follows as a plane wave entering into the system.

$$\mathbf{H}^{\mathrm{inc}} = \begin{pmatrix} 0 \\ 0 \\ 1 \end{pmatrix} \sqrt{\frac{\varepsilon_1}{\mu_1}} \exp\left(ik_1 \hat{\mathbf{k}} \cdot \mathbf{r}\right), \tag{1}$$

$$\mathbf{r} \equiv \begin{pmatrix} x \\ y \\ z \end{pmatrix}, \hat{\mathbf{k}} \equiv \begin{pmatrix} \cos\phi \\ \sin\phi \\ 0 \end{pmatrix}, k_1 \equiv \omega\sqrt{\varepsilon_1 \mu_1},$$

where ϕ is an incident angle and ω is the frequency of the incident wave. The energy flow of an electromagnetic field is defined as the Poynting vector by

$$\mathbf{S} = \frac{1}{2}\mathrm{Re}\left(\mathbf{E}^* \times \mathbf{H}\right). \tag{2}$$

Here, the symbol * expresses complex conjugate. Energy reflectance is defined by the ratio of the integration s_2 about the plane of incidence of the normal component of the Poynting vector of the scattered wave, to that of the incident wave s_1 as

$$R_{\mathrm{f}} = \left|\frac{s_2}{s_1}\right| = \left|\frac{\iint \mathrm{Re}\left(\left(\mathbf{E}^{\mathrm{scat}}\right)^* \times \mathbf{H}^{\mathrm{scat}}\right) \cdot \mathbf{n} dS}{\iint \mathrm{Re}\left(\left(\mathbf{E}^{\mathrm{inc}}\right)^* \times \mathbf{H}^{\mathrm{inc}}\right) \cdot \mathbf{n} dS}\right|$$
$$= \left|\frac{\iint \mathrm{Re}\left(\left(\mathbf{E} - \mathbf{E}^{\mathrm{inc}}\right)^* \times \left(\mathbf{H} - \mathbf{H}^{\mathrm{scat}}\right)\right) \cdot \mathbf{n} dS}{\iint \mathrm{Re}\left(\left(\mathbf{E}^{\mathrm{inc}}\right)^* \times \mathbf{H}^{\mathrm{inc}}\right) \cdot \mathbf{n} dS}\right|, \tag{3}$$

where $\mathbf{E}^{\mathrm{inc}}$ and $\mathbf{H}^{\mathrm{inc}}$ are the incident electric and magnetic fields respectively, $\mathbf{E}$ and $\mathbf{H}$ the total electromagnetic fields and $\mathbf{E}^{\mathrm{scat}}$ and $\mathbf{H}^{\mathrm{scat}}$ the scattered electromagnetic fields. In calculation of an energy reflection spectrum, the wavelength of the incident wave is taken in the range of 380–785 nm as the wavelength λ in a vacuum. On the numerical implementation, high accuracy of 0.6% in the maximum error of the energy conservation law is realized in this wavelength domain.

3. Numerical Results

The reflection spectrum for the incident angle $\phi = 0°$ is shown in Fig. 5. We can see a large peak at $\lambda \approx 550$ nm and a small subpeak at $\lambda \approx 710$ nm.

Figure 6(a) shows the reflection spectrum for $\phi = 30°$. In this case, a gently-sloping peak is observed at $\lambda \approx 500$ nm, and also a very sharp peak can be seen at $\lambda \approx 475$ nm. The magnification of Fig. 6(a) around the sharp peak is shown in Fig. 6(b).

It is thought that the sharp peak is attributed to the phenomenon called Fano effect (Fano and Rau, 1986). The Fano effect is a phenomenon which a characteristic asymmetrical structure appears in transport property, e.g., a transmission spectrum and a reflection spectrum, when a system has discrete states and continuous states (Kobayashi *et al.*, 2002). It is a quantum-mechanical and/or wavy phenomenon in which resonance and interference take place simultaneously. In this system, the resonance between virtual bound states in the photonic crystal and the incident wave would take place.

4. Multilayer Model with an Effective Dielectric Constant

For a reference, here, we compute the energy reflection spectrum by means of the multilayer model with an effective dielectric constant as Miyamoto and Kosaku (2005). The model is as shown in Fig. 7. The system is assumed to be made by stacking the aqueous layer and the effective

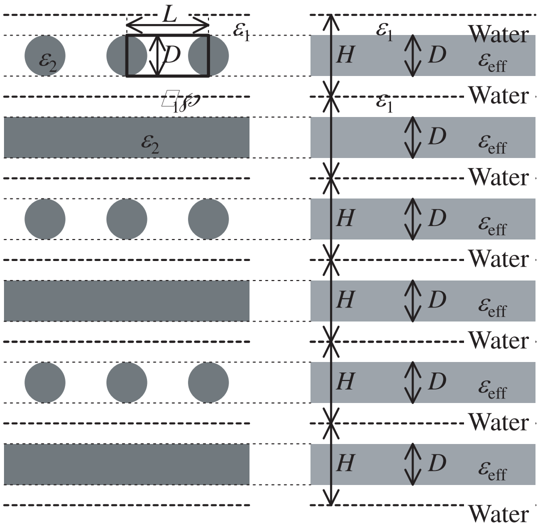

Fig. 7. The multilayer model with an effective dielectric constant $\varepsilon_{\rm eff}$.

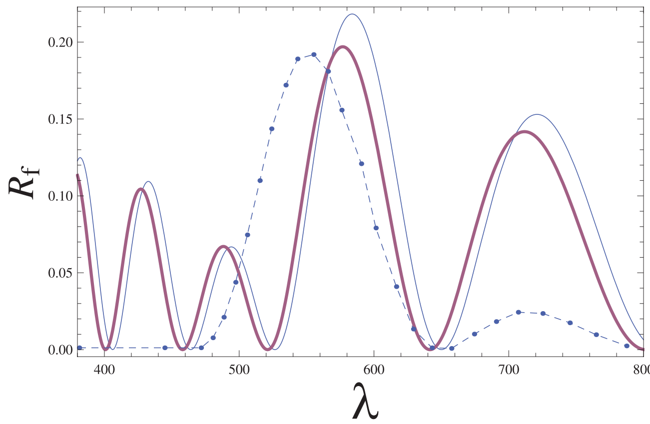

Fig. 8. The energy reflection spectra of the TE mode (solid line) and the TM mode (thick line) computed by the multilayer mmodel for the incident angle $\phi = 0°$. The spectrum of log-pile model is also shown (dashed line).

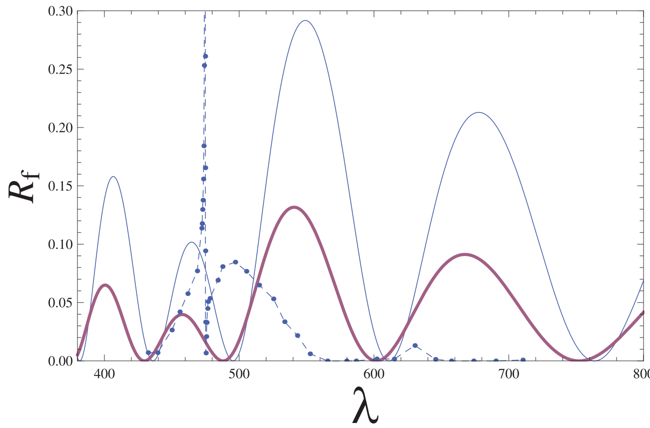

Fig. 9. The energy reflection spectra of the TE mode (solid line) and the TM mode (thick line) computed by the multilayer mmodel for the incident angle $\phi = 30°$. The spectrum of log-pile model is also shown (dashed line).

dielectric layer by turns. An incident wave enters from air. In this model, the reflection spectrum is analyzed about the TE mode and the TM mode, respectively. The electric field in the former and the magnetic field in the latter are parallel to the layer surface. The dielectric constant of an effective dielectric layer for the TE mode is defined by the volume average of the dielectric constant within the fiber layer of a wood pile model as follows:

$$\varepsilon_{\rm eff} = \varepsilon_1 \left(1 - \frac{\pi D}{4L}\right) + \varepsilon_2 \frac{\pi D}{4L}. \tag{4}$$

The value is given as $\varepsilon_{\rm eff} = 2.18791$. The dielectric constant of an effective dielectric layer for the TM mode is, on the other hand, defined by

$$\frac{1}{\varepsilon_{\rm eff}} = \frac{1}{\varepsilon_1}\left(1 - \frac{\pi D}{4L}\right) + \frac{1}{\varepsilon_2}\frac{\pi D}{4L}. \tag{5}$$

The value is obtained as $\varepsilon_{\rm eff} = 2.12569$. We employ a transfer matrix (the interference matrix) method according to Kokubun (1999), in order to calculate the reflection spectrum.

The reflection spectra of both the TE mode and the TM mode in case the incident angle is 0° are shown in Fig. 8. In the case of vertical incidence, the difference between the reflection spectrum of the TE mode and that of the TM mode is not remarkable. Both reflection spectra of the TE and of the TM mode have the highest main peak near the position of the peak in the reflection spectrum of the log-pile model. The height of the peak around $\lambda = 720$ nm of the reflection spectrum of the multilayer model however differs from that of the log-pile model remarkably. The reflection probability of the multilayer model in the domain where wavelength is smaller than 500 nm is remarkably larger than that of the log-pile model.

Figure 9 shows the reflection spectra of both the TE mode and the TM mode for the incident angle $\phi = 30°$. When an incident wave enters at 30°, the reflection probability of the TE mode is, on the whole, much larger than that of the TM mode. The difference between the position of the main peak of the reflection spectrum of the log-pile model and that of the multilayer model grows if an incident angle becomes large.

Thus, when especially an incident angle is not small, a multilayer model is not fruitful and has the numerical computation in which the system is appropriately treated as a photonic crystal is indispensable.

5. Composition of a Structural Color by RGB Color

When we express a color on a computer using the RGB color coordinate system, a color is specified with the tristimulus values R, G and B. Generally, the procedure of calculating the tristimulus values of RGB from a spectrum is as follows (Onai, 2008).

By multiplying a spectrum $R_{\rm f}(\lambda)$ by three color matching functions $\bar{x}(\lambda)$, $\bar{y}(\lambda)$ and $\bar{z}(\lambda)$ of the XYZ color coordinate system, and integrating them with the wavelength λ, the tristimulus values X, Y and Z of the XYZ color coordinate

(a) (b)

Fig. 10. The RGB colors calculated from the reflectance spectra for (a) $\phi = 0^\circ$ and (b) $\phi = 30^\circ$.

(a) (b)

Fig. 11. The RGB colors reproduced by the multilayer model for (a) $\phi = 0^\circ$ and (b) $\phi = 30^\circ$.

system are expressed as follows:

$$X = \int_{380\text{nm}}^{780\text{nm}} R_{\mathrm{f}}(\lambda)\bar{x}(\lambda)d\lambda \tag{6}$$

$$Y = \int_{380\text{nm}}^{780\text{nm}} R_{\mathrm{f}}(\lambda)\bar{y}(\lambda)d\lambda \tag{7}$$

$$Z = \int_{380\text{nm}}^{780\text{nm}} R_{\mathrm{f}}(\lambda)\bar{z}(\lambda)d\lambda. \tag{8}$$

In the present paper, CIE (1931) of 2-deg color matching functions in the CVRL Color & Vision database was employed as the three color matching functions $\bar{x}(\lambda)$, $\bar{y}(\lambda)$ and $\bar{z}(\lambda)$ (The Colour & Vision Research Laboratory, 1995).

Next, X, Y and Z in the XYZ color coordinate system are converted into R, G and B in the RGB color coordinate system by means of the following formulae:

$$R = (3.5064X - 1.7400Y - 0.5441Z)/(X + Y + Z) \tag{9}$$

$$G = (-1.0690X + 1.9777Y + 0.0352Z)/(X + Y + Z) \tag{10}$$

$$B = (0.0563X + 0.1970Y + 1.0511Z)/(X + Y + Z). \tag{11}$$

Since the brightness of a monitoring screen is proportional to the about 2.2 to 2.4th power of a RGB value rather than proportional to a RGB value, the gamma correction for this (R, G, B) is performed. Here, the rectified value is defined by $(R', G', B') = (R^{1/2.2}, G^{1/2.2}, B^{1/2.2})$ (Fumoto, 1999). By using the intrinsic function, RGBColor, of Mathematica (Wolfram Research Inc., 1988), we can specify a color in terms of (R', G', B').

Actual calculations give $(X, Y, Z) = (8.65713, 13.3179, 0.8117)$ for the incident angles $\phi = 0^\circ$, and $(X, Y, Z) = (1.02966, 2.28491, 4.39062)$ for $\phi = 30^\circ$. The values of the RGB tristimulus values are, then, given as $(R, G, B) = (-0.357461, 0.463678, 0.548049)$ and $(R, G, B) = (0.29581, 0.751004, -0.0563071)$, respectively. Although each component of RGB color coordinates is originally defined as positive, one or two (never three) of the R, G, B coordinates often can turn out negative like this, which is the reason why the XYZ color coordinate system is introduced. This means that the color lies outside the "gamut" of colors that the monitor can reproduce. The out-of-gamut colors are fixed according to the standard way to add white—equal parts of R, G, and B—just enough to make all components positive, so bringing the color to the border of the gamut (Hamilton, 1999). That is, add $-\min(R, G, B, 0)$ to each of R, G, and B. Thus, we obtain $(R', G', B') = (0, 0.91432, 0.955886)$ for the incident angles $\phi = 0^\circ$ and $(R', G', B') = (0.622227, 0.907289, 0)$ for $\phi = 30^\circ$. By substituting these values into the function RGBColor of Mathematica, the RGB colors for the incident angles $\phi = 0^\circ$ and $\phi = 30^\circ$ are obtained, and shown in Figs. 10(a) and (b), respectively.

In the case of the incident angle $\phi = 30^\circ$, the structural color of light blue has appeared, which is very similar to one seen in Fig. 2(a).

Performing the same calculation for the TM mode of the multilayer model, we obtain values of (R', G', B') for the incident angle $\phi = 0^\circ$ and for $\phi = 30^\circ$ as $(0.84238, 0.663262, 0.310623)$ and $(0.390027, 0.837913, 0.35026)$, respectively. The colors reproduced in terms of these are shown in Figs. 11(a) and (b), respectively. We see that the reflected light never assumes a color close to a light blue in the multilayer model, whereas the log-pile model can reproduce the structured color.

6. Conclusions

Optical property of the log-pile structure of fibers as a model of the epidermis of an earthworm has been studied by means of the numerical method for photonic crystals. The reflection spectra for several incident angles have been calculated, from which the structural color reproduced in terms of the RGB color for each incident angle. The RGB color calculated from the reflection spectrum for the incident angle $\phi = 30^\circ$ has reproduced the structural color observed on the epidermis of an earthworm very well. This fact clearly shows that the light blue which Kosaku and Miyamoto (2002a, b) observed on the epidermis of an earthworm is attributed to the log-pile structure of fibers.

The difference between the reflection spectra of the multilayer model and the log-pile model becomes remarkable as an incident angle becomes large. It has been confirmed that the multilayer model is not fruitful if the incident angle is not near right angle.

In order to compare in detail, however, it is necessary to measure the reflectance spectrum of the epidermis of an earthworm and to compare it with the ones calculated here. About numerical computation, only the reflection spectrum of the TM mode has been considered in the present paper. It is necessary to perform the same calculation for the TE mode. We would report on these elsewhere in the near future.

Acknowledgments. One of authors, TU, would like to express his special thanks to professor N. Tsumura of Chiba University for instructing him in the conversion method from a spectrum to a RBG color. He also appreciates K. Miyamoto and A. Kosaku of Dokkyo University School of Medicine to presentation of an opportunity of this research and to offer of their observation photographs.

References

Biró, L. P., Bálint, Zs., Kertész, K., Vértesy, Z., Márk, G. I., Horváth, Z. E., Balázs, J., Méhn, D., Kiricsi, I., Lousse, V. and Vigneron, J.-P. (2003) Role of photonic-crystal-type structures in the thermal regulation of a Lycaenid butterfly sister species pair, *Phy. Rev. E*, **67**, 021907.

Fano, U. and Rau, A. R. P. (1986) *Atomic Collisions and Spectra*, Academic Press.

Fumoto, I. (1999) Colors & Dyeing Club in Nagoya/Osaka Web Site, http://www005.upp.so-net.ne.jp/fumoto/linkp25.htm (in Japanese).

Goto, S. and Hatai, S. (1899) New or imperfectly known species of earthworms. No. 2, *Annot. Zool. Japon*, **3**(1), 13–24.

Hamilton, A. (1999) Andrew Hamilton Web Site, http://casa.colorado.edu/ ajsh/colour/rainbow.html

Joannopoulos, J. D., Meade, Robert, D. and Winn, J. N. (1995) *Photonic Crystals: Molding the Flow of Light*, Princeton Univ. Press.

Kinoshita, S. and Yoshioka, S. (eds.) (2005) *Structural Colors in Biological Systems*, Osaka Univ. Press.

Kinoshita, S., Yoshioka, S. and Kawagoe, K. (2002a) Mechanisms of structural colour in the Morpho butterfly: cooperation of regularity and irregularity in an iridescent scale, *Proc. R. Soc. Lond. B*, **269**(1499), 1417–1421.

Kinoshita, S., Yoshioka, S., Fujii, Y. and Okamoto, N. (2002b) Photo-Physics of structural color in the morpho butterfiles, *Forma*, **17**(2), 103–121.

Kobayashi, K., Aikawa, H., Katsumoto, S. and Iye, Y. (2002) Tuning of the fano effect through a quantum dot in an Aharonov-Bohm Interferometer, *Phys. Rev. Lett.*, **88**, 256806–256809.

Kokubun, Y. (1999) *Light Wave Engineering*, Kyoritsu Shuppann, 110–115 (in Japanese).

Kosaku, A. and Miyamoto, K. (2002a) Structural color observed on the surface of annerida, *J. Soc. Sci. Form*, **17**(2), 121–122 (in Japanese).

Kosaku, A. and Miyamoto, K. (2002b) Society for Science on Form, Japan Web Site, http://nkiso.u-tokai.ac.jp/form/event/ssf/sympo54/struct_color/struct_color.htm (in Japanese).

Miyamoto, K. and Kosaku, A. (2005) Fiber structure in epidermis colored earthworm, Lugworm (Annelida) Surface, *J. Soc. Sci. Form*, **20**(2), 167–168 (in Japanese).

Nishiyama, E., Matsuda, T., Itoh, H. and Shimoda, M. (2000) Numerical analysis of structural coloration of wing-scales of morpho butterflies, *Proc. of Application of Electromagnetic Phenomena in Electrical and Mechanical System*, Adelaide, No. 6-2.

Ohtaka, K., Ueta, T. and Amemiya, K. (1998) Calculation of photonic bands using vector cylindrical waves and reflectivity of light for an array of dielectric rods, *Phys. Rev. B*, **57**(4), 2550–2568.

Onai, R. (2008) *Multimedia Computing*, Corona Publ., 77–89 (in Japanese).

Otani, Y. and Nishimura, N. (2008) A periodic FMM for Maxwell's equations in 3D and its applications to problems related to photonic crystals, *J. Comp. Phys.*, **227**, 4630–4652.

The Colour & Vision Research Laboratory (1995) CVRL Color & Vision database, www.cvrl.org

Vukusic, P. and Sambles, J. R. (2003) Photonic structures in biology, *Nature*, **424**, 852–855.

Wolfram Research Inc. (1988) Wolfram Research Inc. Web Site, http://www.wolfram.com/